International Journal of Heat and Technology
Vol. 40, No. 1, February, 2022, pp. 247-257
Journal homepage: http://iieta.org/journals/ijht

Numerical Study of the Temperature Effects on Heat Transfer Coefficient in Mini-Channel Pin-Fin Heat Sink

Nabil Bessanane[1,2*], Mohamed Si-Ameur[1], Mourad Rebay[2]

[1] Faculty of Technology/LESEI Laboratory, University of Batna2, 1, Av. Boukhlouf Med Elhadi, Batna 05000, Algeria
[2] ITHEMM Laboratory, University of Reims Champagne-Ardenne, Faculty of Sciences PB1039, Reims 51687, France

Corresponding Author Email: bessanane@yahoo.fr

https://doi.org/10.18280/ijht.400129

Received: 30 December 2021
Accepted: 21 February 2022

Keywords:
heat sink, pin-fin, heat transfer coefficient, reference temperature

ABSTRACT

Pin-fins are frequently used to increase the heat transfer surface and promote turbulent motion, which improves the devices cooling process by enhancing heat dissipation, as in hydrogen fuel cells applications. The application has burst out this last decade and became vital in several industrial devices. The present study is a numerical investigation of flow and heat transfer in rectangular mini-channels (RMC) and pin-fin heatsinks (PFHS). The pin-fins have a diamond shape arranged in segregated disposition (corrugated channel). In order to adequately calculate the heat transfer coefficient within this complex thermal system; several parameters, such as mass flow rate, geometry dimensions, heat flux and reference temperature are extensively examined. The importance in way the reference temperature was calculated was highlighted. A correct estimation of the heat transfer coefficient led to a better optimisation of the cooling process performances. The aim of this study was to elaborate a technique to correctly estimate the temperature difference between the cooler fluid and the heat sink wall, leading to a better approach for heat transfer coefficient estimation. For this purpose, an approach with variable reference temperature (VRT) has been adopted in the calculation of the wall-fluid temperature difference. Flow field and heat transfer are analysed qualitatively (visualisations of sensible zones) and quantitatively (profiles of heat transfer coefficient, heat flux, wall and fluid temperatures...). The numerical procedure has been validated by experimental measurements. The results showed that the proposed approach to calculate the reference temperature leads to a better presentation of the heat transfer coefficient. In addition, new fit function was involved, in particular the variation of the averaged heat transfer coefficient against Reynolds number.

1. INTRODUCTION

Pin-fins are frequently used in cooling devices to enhance heat dissipation by increasing surfaces and promoting turbulence activity. Various types of fins and pin-fins are commonly used for both natural and forced convection heat transfer. The Pin-fins geometrical arrangement and dimensions factors are extensively examined in many research works, as well as thermal-fluid properties, such as Zukauskas and Moores [1, 2], Shkarah et al. [3]. Beside conventional cases, the use of pin-fin heat sinks micro/mini-channels in cooling systems was proven to be more promising and a useful tool to extract heat, in term of heat transfer dissipation in a small volume, as shown by Obot [4], Kandlikar and Grande [5, 6], Bahrami et al [7]. In the literature, many numerical and experimental studies have been carried out to ensure optimum design and high thermal performance [8-10]. The actual average power dissipation is about 100 W/cm^2, and can reach 500 W/cm^2 peak values. This heat sink feature is manufactured with a high thermal conductivity material such as copper with micro-channels and pins implanted either by precision machining or by micro-fabrication technology. The hydraulic diameter dimensions (Dh) of these micro-channels are between 10 and 1000 μm. It's linked to the coolant fluid passage space. There is a wide classification of mini-channels and micro-channels as reported by several research investigations [11]. Furthermore, the machining and measurement difficulties encountered lead to errors related to certain key parameters such as hydraulic diameter or reference quantities. This disadvantage makes the evaluation of the heat sink performance more complicated according to Morini [12]. Evaluation of the cooler temperature reference presents difficulties because of its variation along the channel from inlet to outlet. All this constraints open horizons in the study of heat transfer for better heat exchange in optical cooling systems. A suitable approach was determined to establish a method, which gives a better representation of the local and the averaged heat transfer coefficient, based on an adequate evaluation of averaged quantities (heat flux, temperatures of wall and fluid).Several quantitative numerical simulations of thermal-fluid fields were carried out to evaluate the thermal system performance; Great attention was devoted to the reference temperature effect as well as local and averaged heat transfer coefficient and compared to experimental results. Many flow studies in micro electro-mechanical systems devices have shown unexpected deviations and dissimilar phenomena compared to large conventional scales applications, additional difficulties were encountered when attempting to use the thermal-fluid conventional approach. Jiang and Xu [13] found that the staggered geometries are

more efficient than those with aligned pins, with lower values of pressure drop and low Reynolds number. While the diamond section pins work better than other shapes and offer maximum performance to the higher Reynolds number.

The heat transfer coefficient for this kind of complex geometry (PFHS) is not enough documented in the literature. This is due to the great difficulties encountered during the evaluation of the various parameters and the rareness of appropriate approaches. Despite its simplicity, this coefficient becomes more complicated to be defined in terms of small scale and complex configurations; where the fluid passage size is in the same order as the solid zones (conjugated heat transfer conditions). Consequently, the temperature of the fluid undergoes strong variations. The reference temperature of the fluid was defined in several ways, constant values in simplified form of bulk temperature and variable values. The study of Liu et al. [14] conducted experimental research on thermal characteristics in a micro heat dissipater with diamond-shaped pins. To evaluate the average heat transfer coefficient, they used the arithmetic mean of the two inlet and outlet temperatures as the reference temperature of the fluid. Yang et al. [15] proposed the use of ($\Delta T_m=T_w-T_{bulk}$) as temperature difference to evaluate heat transfer coefficient, where T_{bulk} is the average temperature of the entire volume of the global domain. The logarithmic difference based the inlet and the outlet temperature can lead to unrealistic value in the case of a temperature small error. The work of Mebarki and Rahal [16] showed that the use of the integral method for calculating the bulk temperature is more promising in the case of simple mini-channel heat sinks. Tullius et al. [17], used a temperature noted "near wall" as the fluid temperature reference for all calculation of the heat transfer coefficient, without giving details on their evaluation process of the reference temperature. Yang et al. [18] used temperature difference ($\Delta T_m=T_w-T_{bulk}$). A good agreement is obtained between numerical simulations and analytical results.

Eren and Caliskan [19] have experimentally analysed the effect of grooves in pins on the heat transfer performance of pin-fin heat sinks, they considered a bulk temperature of the fluid equal to the arithmetic mean of the two temperatures at the input and the output.

2. PROBLEM DESCRIPTION

The mini-channel heat sinks considered in this study are used in the cooling process of the Synchrotron SOLEIL components (absorbers, mirrors, monochromators…etc.). SOLEIL, an acronym for "Optimized Source of Intermediate Energy Light's of LURE (Laboratory for the Use of Electromagnetic Radiation)" the research center in Paris (France), a particle (electron) accelerator that produces synchrotron radiation, an extremely powerful source of light that permits exploration of inert or living matter. Two types of mini-channel heat sinks were studied in numerical investigation: the heat sink with diamond pin-fins shape and the heat sink with simple rectangular mini-channels. The staggered pin fins arrangement has been adopted in our study as it is well known in literature to perform a better more heat transfer enhancement [20-22].

The heat sink shape is a parallelepiped (Figure 1). The heat sink length is *L=100 mm* and its width and height are respectively *W=16 mm* and *H=1.6 mm*. All fins have the same height *1.6 mm* and square base dimensions, the fin width *C=1.7 mm* (Figure 2). The top and the bottom of the domain are planes with *3 mm* thickness. The distributor length (inlet) is about *5 mm* and is sufficient for flow establishment. The collector length (output) is equal to *12 mm*; the origin plot is fixed at *5 mm* and the downstream evolution is ends at *105 mm*.

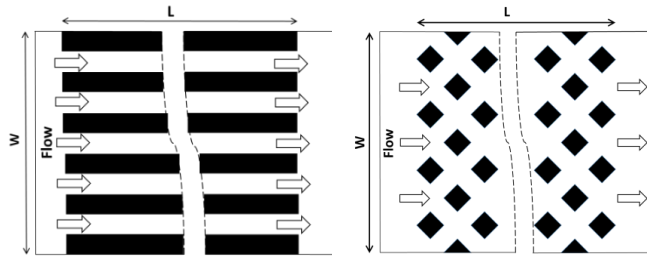

(a) (b)

Figure 1. The heat sink geometries: (a) Rectangular mini-channel (b) diamond pin-fins

In this study, the geometry of the reference dissipater of the type mini-channels is diamond-shaped pins, with the same bulk volume. Different geometries with different fluid passage dimensions (e) were considered; only two cases are presented, which are carried out at different flow rates between (0.05 and 3 *kg/mn*). In addition, an improved near-wall treatment has been introduced because of the very reduced fluid passage, in order to have a better presentation of edge effects on the thermal and hydrodynamic field.

3. PIN GEOMETRY

The pin-fins diamond shape consists of square section (1.7×1.7 mm^2) oriented at a 45° angle in the direction of the flow. Figure 2 shows the fluid passage area for fins geometries: with regular channel (a) and corrugated channel (b). The fins are arranged in staggered configuration which is better from the heat transfer point of view as it mentioned in literature survey, the fluid passage spacing values are (*e=0.35–0.7–1.2* and 1.6 *mm*).

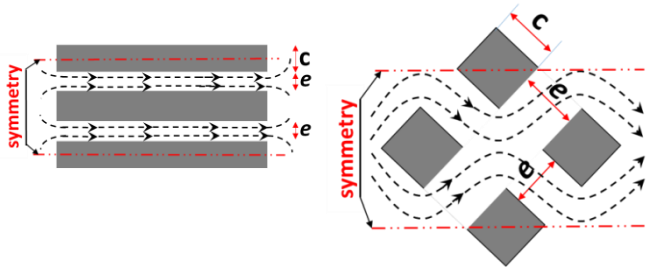

(a): RMC (b): PFHS

Figure 2. Studied configurations shapes Rectangular (RMC) and staggered arrangement for diamond shape (PFHS)

4. MATHEMATICAL FORMULATION AND NUMERICAL APPROACH

4.1 Governing equations

The governing equations for the steady state incompressible flow are given by:

4.1.1 Continuity equation

$$\frac{\partial(\rho U_j)}{\partial x_j} = 0 \tag{1}$$

4.1.2 Momentum and energy equations

$$\frac{\partial(\rho U_i U_j)}{\partial x_j} = -\frac{\partial P}{\partial x_j} + \frac{\partial}{\partial x_j}\left(\mu\left(\frac{\partial U_i}{\partial x_j} + \frac{\partial U_j}{\partial x_i}\right) - \left(\frac{2}{3}\delta_{ij}\mu\frac{\partial U_k}{\partial x_k}\right) - \rho\overline{u_i u_j}\right) \tag{2}$$

$$U_j\frac{\partial(\rho T)}{\partial x_j} = \frac{\partial}{\partial x_j}\left(\frac{\lambda}{C_P}\frac{\partial T}{\partial x_j} - \rho\overline{tu_j}\right) \quad , \quad were: \overline{tu}_j = \nu_t\frac{\partial T_i}{\partial x_j} \tag{3}$$

Eq. (2) is written to represent the dynamical field; the Reynolds stress appears in RANS and is the adequate representation for all cases involved in our study. The convection equation (3) is also written in turbulent regime; temperature and velocity fluctuations are correlated through the new term which appears in the energy equation. The heat conduction process is explicitly taken into account in the solid zone. In this study, the radiation effects are not considered, the Realizable k-ε turbulence model has been used. The thermo-physical properties of the fluid vary according to the polynomial law.

4.2 Boundary conditions

The boundary conditions can be summarized as follows in Figure 3:

- At the inlet, temperature and velocity are imposed; the inlet temperature is fixed to 303°K, while the inlet velocity varies according to the imposed mass flow rate.
- At the outlet, all the variables gradients are fixed to the Newman condition, expected the pressure which is imposed to 3 bars (the nominal parameter given by data experiment).
- A non-slip condition is considered for all inside walls and adiabatic condition is applied to the outside walls.
- A constant heat flux density (*q*) is imposed on bottom base of pins, values given by experimental data.
- Symmetry plans are considered with no heat exchange.
- Conjugate heat transfer conditions were considered at the solid-fluid interface:

$$\begin{cases} q = -\lambda_f\dfrac{\partial T_f}{\partial n} = -\lambda_s\dfrac{\partial T_s}{\partial n} \\ T_f = T_s \end{cases} \tag{4}$$

where, *n* is the vector normal to the boundary.

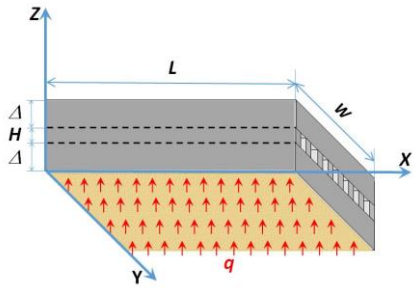

Figure 3. Characteristics of the studied geometry

Figure 3 shows the boundary conditions. It is shown how the heat flux density is imposed on the solid bottom.

Position	***Boundary condition***
z=0	: uniform heat flux *q* at the base plan (x,y)
z=Δ and Δ+H	: fluid-solid conjugate heat transfer conditions
z=2Δ+H	: adiabatic on top plan (x,y)
y=0 and y=W	: adiabatic on lateral plan (x,z)
x=0 and x=L	: adiabatic on plan (y,z)
x=0	: inletvelocity
x=L	: outflow conditions

4.3 Numerical procedures

The numerical calculations were carried out using the ANSYSFLUENT code with finite volume method approach. The simple algorithm was used for pressure–velocity coupling. The second order "Up-wind" scheme is chosen for discretization of the governing equations. Several turbulence models based on RANS are tested. The optimal model is Realizable k-*ε* with “Enhanced-Wall-Treatment”.

The modeled transport equations for *k* and *ε* in the realizable *k-ε* model are:

$$\frac{\partial}{\partial t}(\rho k) + \frac{\partial}{\partial x_i}(\rho k u_i) = \frac{\partial}{\partial x_i}\left[\left(\mu + \frac{\mu_t}{\sigma_k}\right)\frac{\partial k}{\partial x_i}\right] + G_k + G_b - \rho\varepsilon - Y_M + S_k \tag{5}$$

$$\frac{\partial}{\partial t}(\rho\varepsilon) + \frac{\partial}{\partial x_i}(\rho\varepsilon u_i) = \frac{\partial}{\partial x_i}\left[\left(\mu + \frac{\mu_t}{\sigma_\varepsilon}\right)\frac{\partial \varepsilon}{\partial x_i}\right] + \rho C_1 S_\varepsilon - \rho C_2\frac{\varepsilon^2}{k+\sqrt{\nu\varepsilon}} + C_{1\varepsilon}\frac{\varepsilon}{k}C_{3\varepsilon}G_b + S_\varepsilon \tag{6}$$

where: $G_k = \tau_{ij}\dfrac{\partial u_i}{\partial x_j} = \mu_t S^2$, $G_b = \beta g_i\dfrac{\mu_t}{\mathrm{Pr}_t}\dfrac{\partial T}{\partial x_i}$, $\beta = -\dfrac{1}{\rho}\left(\dfrac{\partial\rho}{\partial T}\right)_P$,

$\tau_{ij} = \mu_t\left(2S_{ij} - \dfrac{2}{3}\dfrac{\partial u_k}{\partial x_k}\delta_{ij}\right) - \dfrac{2}{3}\rho k\delta_{ij}$, $S_{ij} = \dfrac{1}{2}\left(\dfrac{\partial u_i}{\partial x_j} + \dfrac{\partial u_j}{\partial x_i}\right)$,

$\mu_t = \rho C_\mu\dfrac{k^2}{\varepsilon}$ $C_1 = \max\left[0.43, \dfrac{\eta}{\eta+5}\right]$ $where: \eta = S\dfrac{k}{\varepsilon}$ and $S = \sqrt{S_{ij}S_{ij}}$

and C_μ isn’t constant as *RNG k-ε* model it’s given by: $C_\mu = 1/A\left(_0 + A_S\dfrac{k}{\varepsilon}U^*\right)$;

A_0, A_S, C_2, $C_{1\varepsilon}$, $C_{3\varepsilon}$, σ_k and σ_ε are constants.

The choice of this model is not arbitrary but it is extracted from several tests in bi-dimensional numerical simulations, the results will be the subject of another scientific paper. Conjugate conduction–convection heat transfer at the fluid–solid interface has also been considered. The physical model configuration is designed in accordance with existing experimental prototypes; and in order to reduce the computation time, the symmetry of the problem has been taken into account in the stream-wise direction.

4.4 Grid independence study

An unstructured mesh has been deployed to present the internal complexity of the geometry, formed by a channel filled with a matrix of pins. The mesh has been adapted to assure satisfactory resolution coverage: close to the "adhesion" walls where the velocity gradients and temperature are expected to be large and to detect the flow velocity variation

due to the decrease of the fluid passage cross-section between pins. Between one and two million nodes were used to generate the entire mesh of the computational domain.

A grid independence study was carried out to assure no influence of mesh on the simulation results. The grids were adopted on the difference of the heat transfer coefficient and the fluid temperature and the effects between the two which remained less than 2%. The average fluid temperatures in channel for typical case are shown in Table 1. It can be seen that the averages quantities deviations are about 1,631,060 nodes compared to the grids with 1,205,954 nodes are 0.3%, 0.1% and 1.7% respectively. The difference between these two grids is less than 2%. Furthermore, the size of the neighbouring elements at the walls has been gently refined, introducing the improved near-wall treatment to ensure a better accurate resolution of any gradient in this region (Figure 4). We confirmed that the mesh refinement is limited to a threshold to get independent solutions. If we continue to refine, the truncation error will be amplified, the solutions will no longer make sense physically.

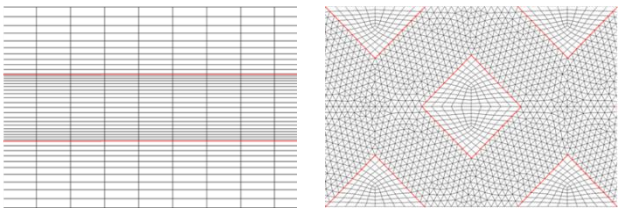

(a) *RMC* (b)*PFHS*

Figure 4. Geometries Mesh: (a) rectangular (b) Diamond fins

Table 1. Heat transfer coefficients, bulk and outlet fluid temperatures for different grids

Parameters	Grids 803,520	Error %	Grids 1,224,860	Error %	Grids 1,631,060
h_{ave} (W/m^{2}K)	3670	6.1%	3421	1.7%	3364
T_{ave} (K)	347.2	0.5%	345.6	0.3%	346.5
T_{out} (K)	358.2	0.2%	357.6	0.1%	357.1

4.5 Parameters and data treatment

The inlet Reynolds number was calculated according to the mass flow rate for each simulation. The Reynolds number in the fluid passage zone between the pins was treated specifically with great attention to estimate of the maximum velocity. A special treatment to obtain U_{max} based on the correct estimation of the hydraulic diameter as defined below. It is important to note that the coefficient factor between our approach and M. Liu approach [13] is about $\sqrt{2}$.

Our approach follows exactly the flow path between pins when the control surface taken is $e \times H$, perpendicular to the flow direction (Figure 2). The maximum velocity is calculated at the smallest cross section of the fluid passage, inside the channel embedded with pin-fins array.

$$\mathrm{Re} = \frac{U_{\max} D_h}{\nu} \quad \text{and} \quad D_h = \frac{2eH}{e+H}$$

The hydraulic diameter is defined with respect to the rectangular section of the fluid passage between fins, with a height (H) and a width (e). The new approach to compute the heat transfer coefficient elaborated in this research is as follows:

- The local faces heat transfer coefficient is defined as:

$$h(x) = \frac{q_w(x)}{T_w(x) - T_f(x)}$$

where: $q_w(x)$ is the local heat flux density at the interface surface, $T_w(x)$ the local temperature at the end wall interface of pin and $T_f(x)$ the local temperature of the fluid at channel axis opposite to a pin face.

- The face-average heat transfer coefficient is defined as:

$$h_{ave}(i) = \frac{q_{w,ave}(i)}{T_{w,ave}(i) - T_{f,ave}(i)}$$

where: $q_{w,ave}(i)$ is the local average heat flux for a pin face, $T_{w,ave}(i)$ the local average temperature at the end wall interface of a pin face and $T_{f,ave}(i)$ the local average fluid temperature at channel axis (the middle face) for the face opposite to the pin face (see Figure 5). All these quantities are computed for each pin face at different streamwise positions (i) along the channel axis.

- The global average heat transfer coefficient for the channel is given by:

$$\bar{h} = \frac{1}{N} \sum_{1}^{N} h_{ave}(i)$$

where, $\bar{h}$ is taken as the average of all (N) faces and it corresponds to a fixed value of mass flow rate; N is the number of pins in stream-wise direction. There are two kinds of faces for each pin (front and back), which lead to compute separately the heat transfer coefficient in front-side and back-side ($\bar{h}_{front}$ and $\bar{h}_{back}$) in stream-wise direction as shown in Figure 5. $\bar{h}_{front}$ and $\bar{h}_{back}$ are calculated by taking into account; the top, the bottom and the two lateral faces for each channel (Figure 6), using:

$$h_{ave}(i)\big|_{front} = \frac{1}{4}\left(h_{top,i} + h_{bottom,i} + 2h_{lateral,i}\right)\Big|_{front}$$

$$h_{ave}(i)\big|_{back} = \frac{1}{4}\left(h_{top,i} + h_{bottom,i} + 2h_{lateral,i}\right)\Big|_{back}$$

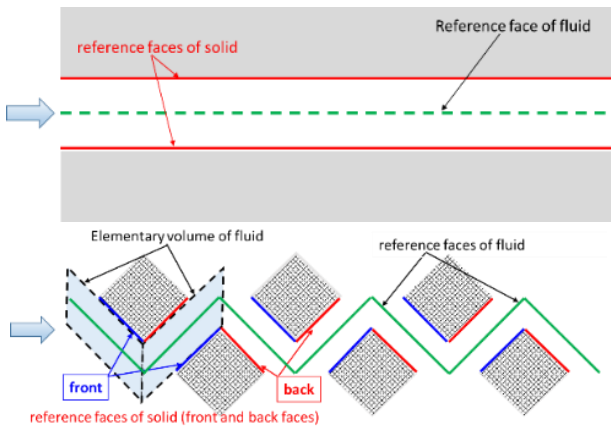

Figure 5. Fluid reference faces and solid zones

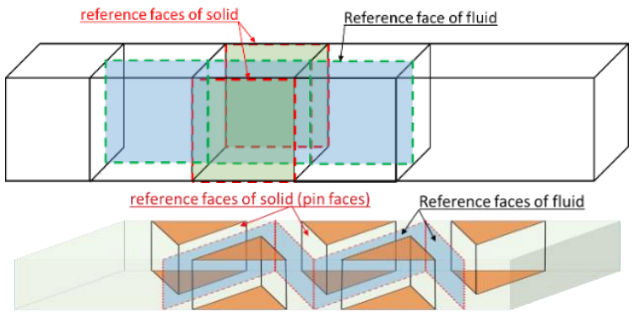

Figure 6. Two channels: RMC regular and PFHS corrugated

Both local and average Nusselt numbers are defined based on the hydraulic diameter and the heat transfer coefficient (local and average):

$$Nu_x = \frac{h_x D_h}{\lambda_f} \ , \ Nu_{ave} = \frac{h_{ave} D_h}{\lambda_f}$$

where, λ_f is the coolant conductivity.

5. RESULTS AND DISCUSSION

Numerical simulations were carried out for two configurations; rectangular mini-channel (RMC) and pin-fins diamond shaped heat sink (PFHS). The results are presented corresponding to different mass flow rates and different geometry dimensions.

5.1 Numerical procedure validation

To validate our numerical procedure, the heat sink pressure drop results and heat transfer coefficient were compared to experimental results from the literature. Figures 7 and 8 show respectively, the comparison of experimental results obtained in synchrotron SOLEIL by Rebay et al. [23] and those obtained by Liu et al. [14]. The results are given for different Reynolds number and for different width (*e*). It can be clearly seen that they are in good agreement.

The average heat transfer coefficient from the numerical procedure was compared to those obtained experimentally in Synchrotron SOLEIL by [23]. From Figure 9 a good agreement is reached for PFHS case with *e=0.35 mm*.

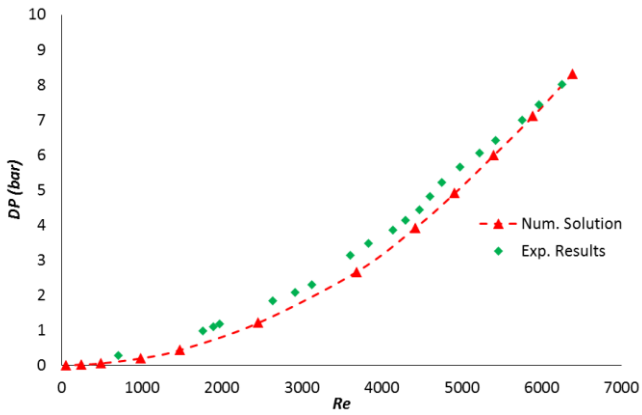

Figure 7. Numerical pressure drop vs. Re (*e=0.35 mm*) for *PFHS* compared to experimental data [23]

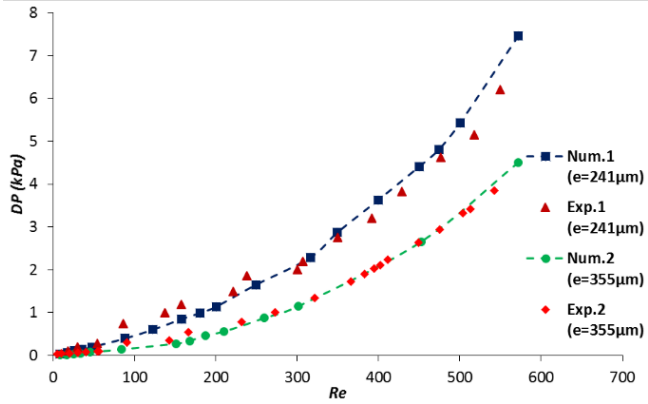

Figure 8. Numerical **p**ressure drop vs. Re for *PFHS* compared to experimental data [14]

From this comparative study, we can conclude that our numerical simulation procedure has been validated, and consequently, further parametric studies may be carried out.

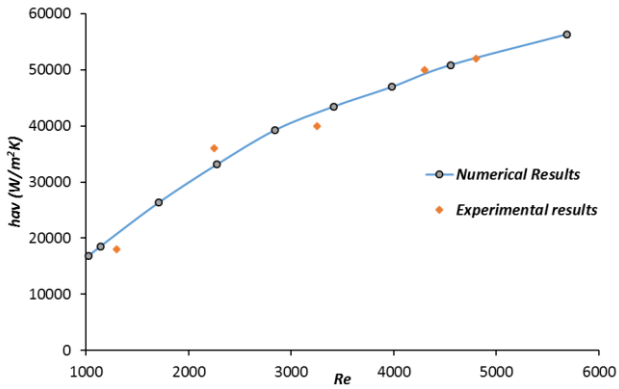

Figure 9. Numerical averaged heat transfer coefficient compared to experimental data [23]

5.2 Results

Local heat transfer coefficient variation for diamond pin-fins heat sink is presented in Figure 10; a zigzag curvature appears because of the periodic alternation of front-back sides and discontinuities between pins. The higher peaks correspond to front sides of pins and the lower to their back sides, along a line of pin-fins in streamwise direction. It can also be seen that, the classic appearance of the local heat transfer coefficient is found, in both cases of RMC and PFHS.

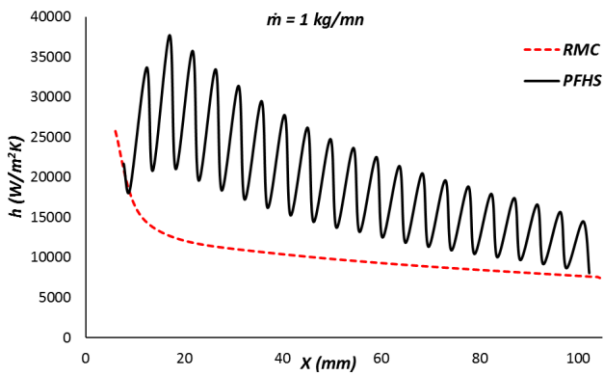

(a) e = 1.6 mm, ṁ=1 kg/mn,Re$_c$ =2300, Dh$_c$=1.6 mm

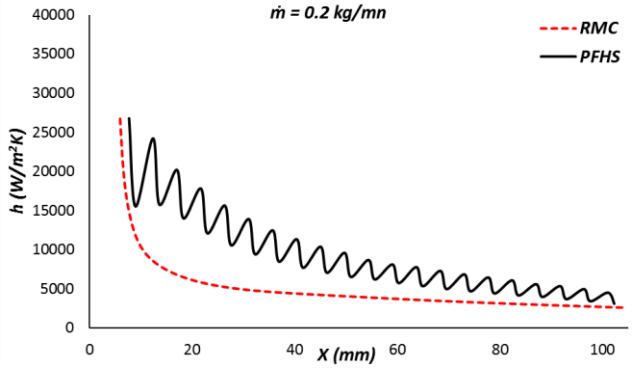

(b) *e=1.6 mm,ṁ =0.2 kg/mn,Re$_c$ =132, Dh$_c$=1.6 mm*

Figure 10. Local heat transfer coefficient along the PFHS and the RMC configuration (*q =100 kW/m^2*)

The static temperature contours are presented in Figure 11, it is clear that the colder areas of the fluid are always located at the central region of the channel. Going from the inlet to the exit this zone is overheated progressively and the reference temperature will change in the streamwise direction. This involves the variation of the temperature difference between fluid and wall to be larger and take its maximum values along the channel. So, the choice of middle faces as reference area allowed to have lower values of fluid temperature and then to keep a temperature difference $\Delta T_m=T_w-T_f$ to assure the existence of a heat flux exchange at the wall until thermal stability is reached (thermal equilibrium $T_f=T_w$). Furthermore, this middle area presents the ideal region where hot and cold fluids are well mixed, it is the area where the wakes are more important and the flow is strongly accelerated to promote a good fluid mixture, as shown in Figure 11.

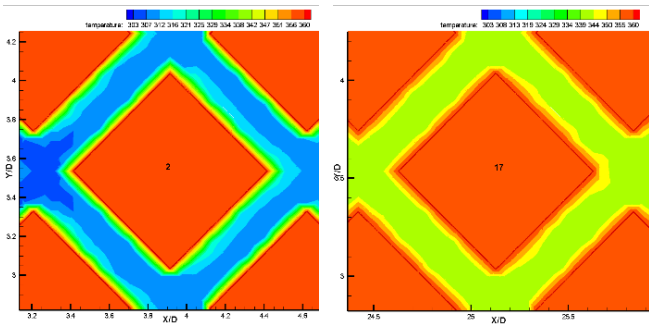

(a)2nd pin (b) 17th pin

Figure 11. Static temperature contours for PFHS (*e=0.7 mm*)

Figure 12 shows contours of velocity magnitude at low mass flow rate (ṁ=1 *kg/mn*) and at passage section with *e=1.2 mm*. It can be observed that the flow is accelerated periodically near the front edge. In the red region, the fluid is accelerated due to the flow narrowing section, because of the large number of recirculation zone as it is clearly observable in Figure 12. The wake region is important between fins in the lozenge configuration. However, the flow topology is capable to mix rapidly the hot and cold temperatures and can lead to heat transfer enhancement with the disadvantage of a rise in pressure drops related to this type of complex geometry.

In Figure 13, the staggered arrangement caused a larger flow resistance than the in-line arrangement with pin-fins. The recirculation regions are remarkably important in back region fins case. The recirculation zones start after the wake region then elongated downstream of pin-fins. This allows lower mixing of the fluid shear layer in back region which leads to low heat transfer rate.

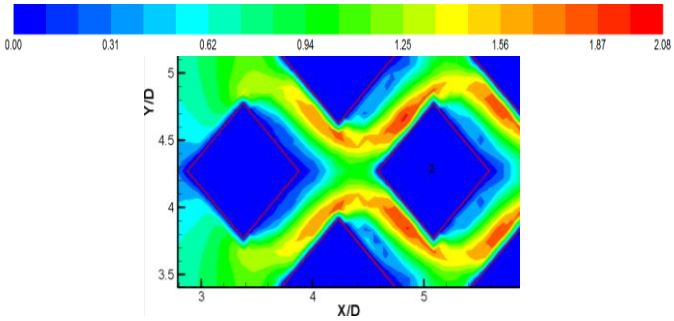

Figure 12. Contours of velocity magnitude (m/s) with (e=1.*2 mm* and *ṁ=1 kg/mn*)

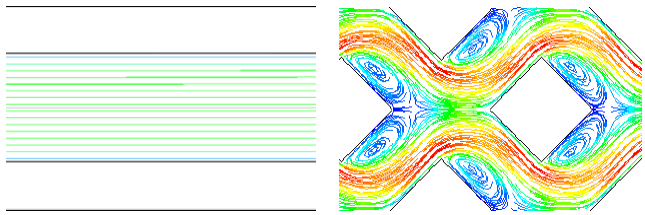

(a) RMC (b) PFHS

Figure 13. Stream lines colored according to velocity magnitude (m/s) with *ṁ*=1 *kg/mn*

5.3 Fluid reference temperature effects

In this part of the work, anew description was used to present reference parameters involved in the calculation of the heat transfer coefficient. These quantities are linked to reference faces for both fluid and pin wall such as presented above in Figures 5-6. This allows taking into consideration the fluid temperature variation along the channel, leading to a better evaluation of the heat transfer coefficient. Figures 14 and 15 illustrate the temperature distribution for the same conditions, on vertical plan (*xy*) and horizontal plan (*xz*) at y=1%, 50% and 99% of *H* for the rectangular mini-channels heat sink and diamond pin-fins heat sink respectively. It can be observed that, the temperature increased along the stream-wise direction due to heat transfer from the base wall with constant applied heat flux (*q = 100 kW/m^2*). In addition, it can be seen that the pins play an important role in mixing the hot and cold fluid therefore increasing the heat transfer rate. Furthermore, it is evident that low fluid temperatures are always located along the channels axis (fluid passage), that is the argument for which the temperature difference will reach maximum values ($\Delta T = T_w-T_f$). The reference temperature ($T_{ref}=T_f$) can be taken at channel axis; varying from the inlet to the outlet $T_{ref}(x)$. This approach will be used in the calculation of the reference temperature, which is more suitable in our method to evaluate the average heat transfer coefficient.

The fluid temperature in plane *xz* (Figure 14) increases sensibly from 303 K to 369 K at the mass rate of *0.05 kg/mn*, the wall temperature reaches 356 K. However, in the *xy* plane at y = 0.99 H, the temperature difference is significant from the inlet to the outlet and between wall and fluid at the outlet. Keeping the difference temperature at a certain level along the heat sink is important in term of heat sink performance. Thus, in mini-channel, the highest temperature difference is obtained

for the higher mass flow. For the pin fins heat sink (Figure 15), the fluid temperature in plane *xz* increases significantly from 303 K to 350 K at the mass rate of 0.05 kg/mn, the wall temperature reaches 356 K. In the *xy* plane at y = 0.99 H and y = 0.5 *H*, the temperature difference is significant from the inlet to the outlet and between wall and fluid at the outlet. The improved cooling is obtained in *xy* plane at y=0.5 *H*.

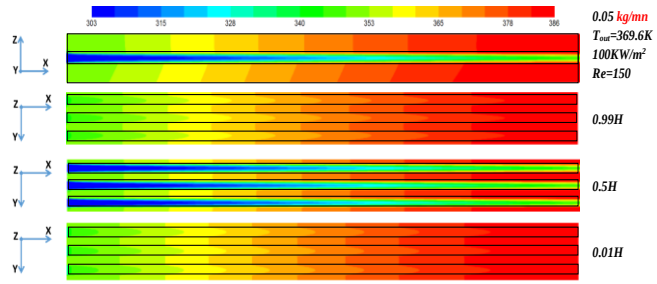

Figure 14. Temperature contour at longitudinal plan for RMC (*e=1.6 mm and ṁ=0.05 kg/mn*)

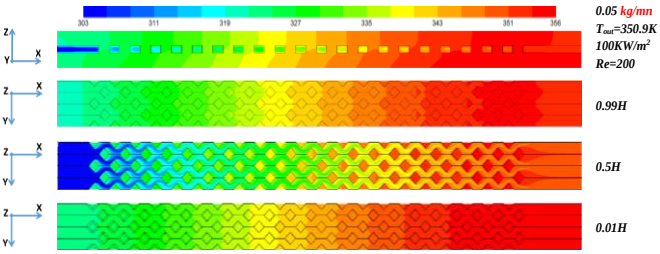

Figure 15. Temperature contour at longitudinal plan for PFHS (*e=1.6 mm and ṁ=0.05 kg/mn*)

The best estimation of the heat sink thermal performances is based on the adequate computation of the average heat transfer coefficient, which is strongly linked to the fluid temperature reference T_{ref}. Several approximations were used to approach this temperature; we define:

- Inlet temperature: $T_{ref} = T_{in}$
- Average temperature of the channel volume: $T_{ref} = T_{bulk}$
- Average arithmetic temperature of inlet-outlet: $T_{ref}=(T_{out}+T_{in})/2$
- Average local temperature vs. (*x*): $T_{ref}=T_{ave}(x)$

Figure 16 shows a comparison of fluid temperature profiles along the channel. It is clear that, both fluid reference temperatures $T_{out\text{-}in}$ and T_{bulk} start with values higher than the wall temperature. However, the inlet fluid temperature must be less than the fluid temperature at the wall (cooler fluid). Furthermore, the wall temperature profile increases along the canal and intersects the$T_{out\text{-}in}$ and T_{bulk} profiles. At these intersections, the wall and fluid temperatures are equal, giving $\Delta T=0$, which gives indeterminate values of heat transfer coefficient. When the reference temperature is taken equal to T_{in}, the wall-fluid temperature difference ΔT increases continually from the inlet to the outlet. This temperature difference is supposed to decrease, because of the wall-fluid heat transfer along the channel. It is obvious that these three reference temperature approximations ($T_{out\text{-}in}$, T_{in} and T_{bulk}) must be ignored. If the reference temperature is equal to the one we adopted, based on the local average fluid temperature in the middle of the channel ($T_{ref}=T_{ave}(x)$), then the temperature difference ΔT_m is higher at the inlet followed by a progressive decrease until that T_w and T_f become close to each other. A low value of ΔT_m indicates that, the cooling process was carried out adequately.

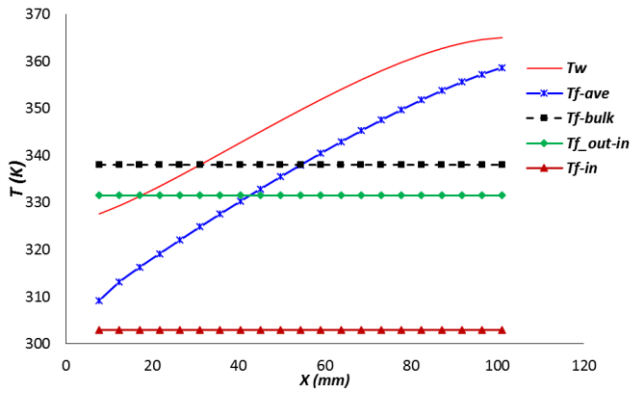

Figure 16. Comparison of different fluid reference temperatures for PFHS (*e=1.6 mm and ṁ= 0.04 kg/mn*)

The local heat transfer coefficient is illustrated in Figure 17 for different reference temperatures approaches. It is evident that the approached local heat transfer coefficient is unsatisfactory when using $T_{out\text{-}in}$ *and* T_{bulk}, a discontinuity is observed at x = 17 and x = 31 respectively (corresponding to $\Delta T=0$). On the other hand, the local heat transfer coefficient tends to very low values at the heat sink outlet for the three different approaches ($T_{out\text{-}in}$, T_{bulk} and T_{in}). The profile of the heat transfer coefficient, as known in the literature, begins with a high value and decreases to an asymptotic value corresponding to the well-established thermal regime. This is the case of the local heat transfer coefficient calculated with a reference temperature taken equal to $T_{ave}(x)$.

Figures 18, 19, 20 and 21 show the pin fin heat sink fluid and wall heat flux and local temperature for fluid passage dimensions *e=1.6 mm* and *e=0.35 mm*. The local temperature is estimated on the basis of averaging the temperatures on front and back fluid passage axis (see reference faces in Figures 5-6). We can clearly observe the intermittent character of the total heat flux along the heat sink, between front and back faces of pin fins. The high values of heat flux are detected in the front faces of the pins; however, the low values are obtained for the back faces regions. The back pin regions are not completely exposed to the fluid flow and several recirculation zones are observed (Figure 13b). These zones are not favorable to heat transfer convection.

Figure 22 shows the local heat transfer coefficient profiles for bottom, top and lateral faces of the rectangular mini-channel and pin-fin heat sinks. The calculations were performed using our fluid reference temperature approach, with an applied constant heat flux $q=100\ kW/m^2$ and a mass flow rate $\dot{m}=1\ kg/mn$. It is clear that, for the mini-channel, the same profile is obtained for all faces, beginning with high values and decreasing to the constant values at the outlet corresponding to the well-established thermal regime. Furthermore, for the pin-fins case, a difference is observed between these profiles. The heat transfer coefficient begins with low values at the inlet and then increase along the geometry to reach a constant value until the outlet, due to the vortex generated by the fins. On the other hand, strong oscillations are observed in the lateral surface compared to other surfaces.

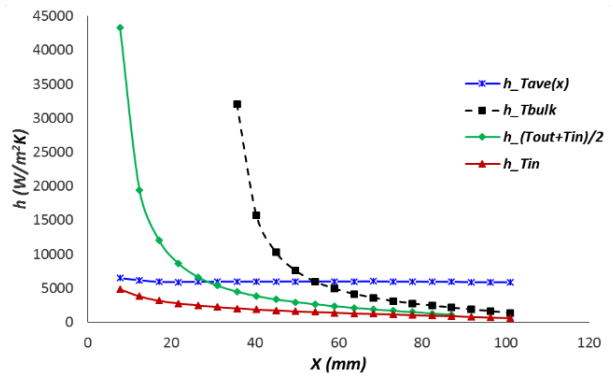

Figure 17. Comparison of local heat transfer coefficients with different methods (*e = 1.6 mm, q=100 kW/m² and ṁ=0.04 kg/mn*)

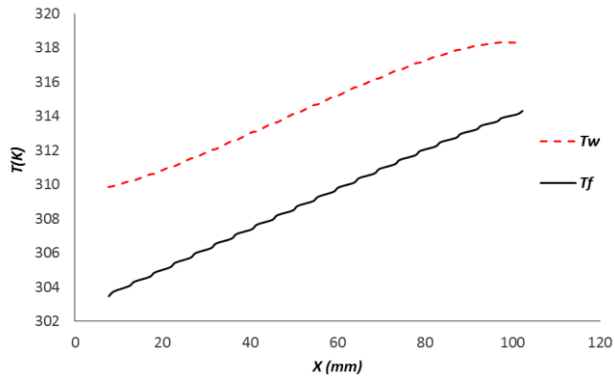

Figure 18. Fluid and wall local temperature for *e = 1.6 mm and ṁ = 0.2 kg/mn*

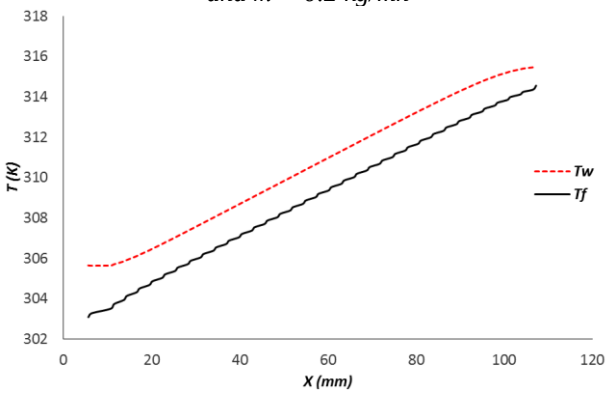

Figure 19. Fluid and wall local temperature for *e = 0.35 mm and ṁ = 0.2 kg/mn*

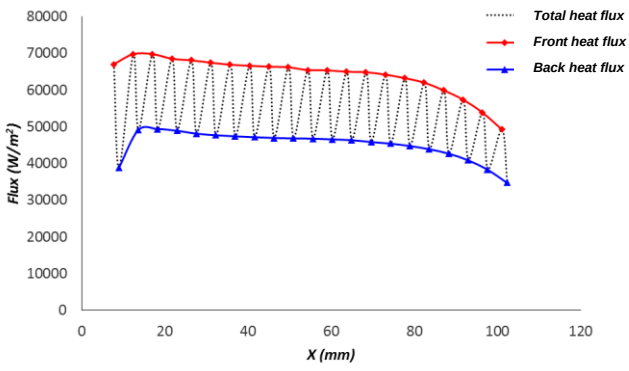

Figure 20. Total, front and back heat flux for*e = 1.6 mm an dṁ = 0.2 kg/mn*

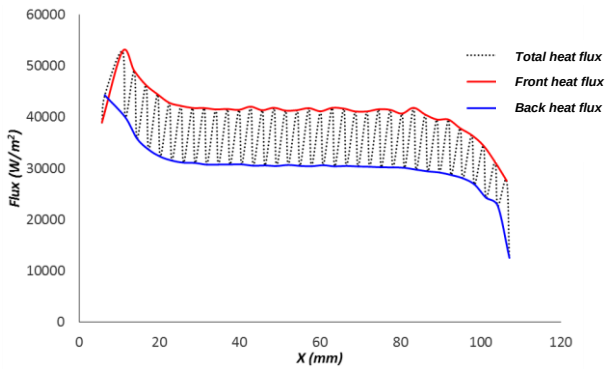

Figure 21. Total, front and back heat flux for*e = 0.35 mm and ṁ = 0.2 kg/mn*

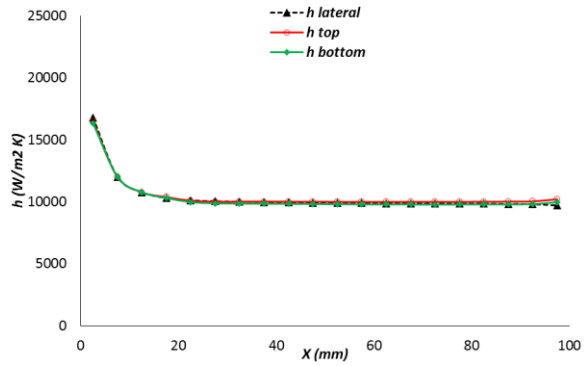

(a) RMC

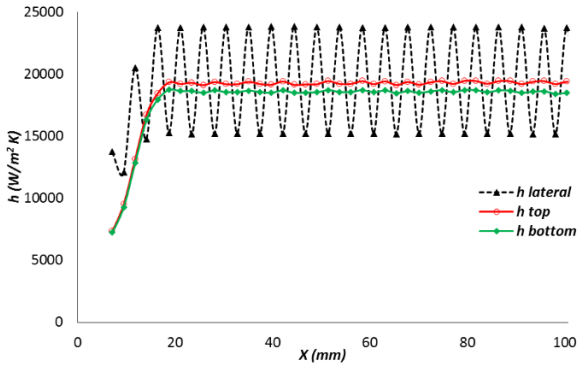

(b) PFHS

Figure 22. Local heat transfer coefficient for *e=1.6 mm and ṁ = 1 kg/mn*

Figure 23 shows the local heat transfer coefficient profiles for different flow rates, using our fluid reference temperature approach. *H* was calculated for the lateral faces for both mini channels and pin-fins heat sink. The results show, as expected, that the heat transfer coefficient increases with mass flow rates and then with Reynolds number.

Averaged heat transfer coefficient fit function:

A fit functions are developed for the two studied configurations to present the averaged heat transfer coefficient profiles as function of Reynolds number based on our reference temperature approach $T_{ave}(x)$. In the comparison presented in Figure 8, the obtained heat transfer coefficient is in good agreement with the experimental measurements of Rebay et al. [23]. The fit functions are developed in simplified form, which can be useful for engineering applications. The proposed correlations are illustrated in Figure 24. It can be seen that the proposed functions represent correctly the numerical results.

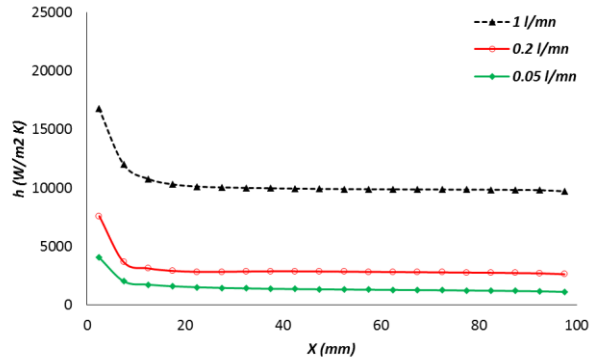

(a)RMC

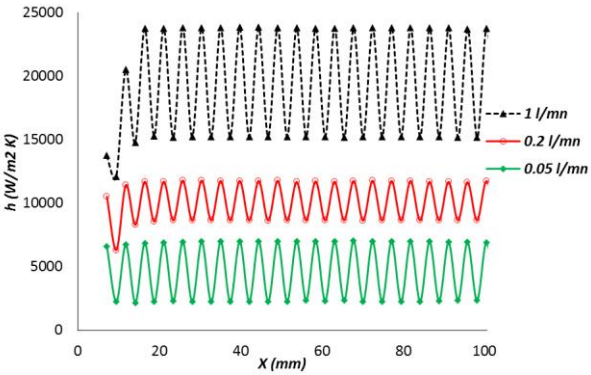

(b)PFHS

Figure 23. Local heat transfer coefficient for different flow rates (*q=100 kW/m² and e = 1.6 mm*)

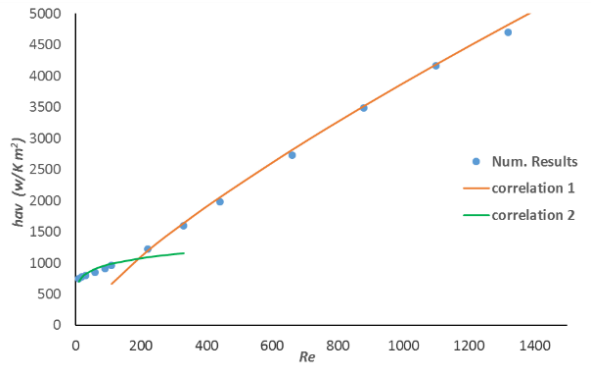

a) h_{ave} based on $T_{ave}(x)$ for RMC (e=1.6 mm)
correlation 1: $h_{ave}= 17\ Re^{0,780}$
correlation 2: $h_{ave}= 504\ Re^{0,143}$

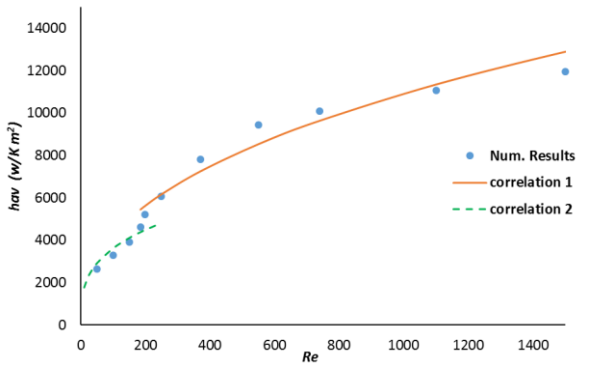

b) h_{ave} based on $T_{ave}(x)$ for PFHS (e=1.6 mm)
correlation 1: $h_{ave}= 634\ Re^{0,412}$
correlation 2: $h_{ave}= 870\ Re^{0,310}$

Figure 24. Heat transfer coefficient vs Re (a) RMC (b) PFHS

6. CONCLUSIONS

A numerical study of flow and heat transfer in rectangular mini-channels and diamond shaped pin-fin heat sinks is carried out. A deep analysis is performed in order to show the influence of fluid reference temperature variation on heat transfer coefficient calculation in such complex geometry. The importance of the manner in which this reference temperature was calculated was highlighted, through different evaluation methods of the fluid reference temperature. The numerical procedure has been validated against experimental measurements and a good accord has been obtained. From the present results, the following points can be drawn as follows:

1) A specific allure (zigzag curvature) of heat transfer coefficient profile has been found based on the variation caused by the front and the back faces of pin-fins. In addition, the classic appearance of the local heat transfer coefficient is well found for both cases of RMC and PFHS.

2) The colder areas of the fluid are always located at the central region of the channel. Therefore, the wall-fluid temperature difference is preserved along the channel. This assures that a heat transfer rate is maintained from the inlet to the outlet.

3) The pin-fins heat sink thermal performances are better than those of the rectangular mini-channels even at lower mass flow rates with acceptable pressure drop values.

4) It can underline that variable fluid reference temperature (VRT) approach reproduce adequately the concept of the well-known T_{∞}, as it is the low fluid temperature at the position far enough from the wall.

5) With this new VRT approach, the profile of heat transfer coefficient maintains a constant form, which gives a better explanation from the point of view of heat transfer improvement; this reflects a closer presentation of the physical aspect. In other terms, the other methods used to compute the fluid reference temperature produce higher and exaggerated values of heat transfer coefficient, especially at the entrance boundary. Furthermore, the heat transfer coefficient reaches low values at the exit boundary. This behaviour is in contradiction with the physical reality to improve the heat transfer by using pin-fins in heat sinks.

6) In practice, the layout of a diamond shaped pin-fin heat sink is shown to be important for its cooling capacity.

Thermal performance of this complex configuration is extremely closed to the correct evaluation of the heat transfer coefficient. It is shown that the variation of the fluid temperature is a key factor and the open door to adequately compute the h coefficient and then the global performance of the heat sink. As the author's knowledge, this work can be seen as first work for a rigorous estimation of heat transfer coefficient in such complicated geometry. In addition, heat transfer coefficient correlations will be developed in future works.

REFERENCES

[1] Zukauskas, A. (1972). Heat transfer from tubes in crossflow. Advances in Heat Transfer, 8: 93-160. https://doi.org/10.1016/S0065-2717(08)70038-8

[2] Moores, K.A., Joshi, Y.K. (2003). Effect of tip clearance on the thermal and hydrodynamic performance of a shrouded pin fin array. J. Heat Transfer, 125(16): 999-1006. 99-1006. https://doi.org/10.1115/1.1621897

[3] Shkarah, A.J., Sulaiman, M.Y.B., Ayoba, M.R.B.H., Togun, H. (2013). A 3D numerical study of heat transfer in a single-phase micro-channel heat sink using graphene, aluminum and silicon as substrates. International Communications in Heat and Mass Transfer, 48: 108-115. https://doi.org/10.1016/j.icheatmasstransfer.2013.08.006

[4] Obot, N.T. (2002). Toward a better understanding of friction and heat/mass transfer in microchannels-A literature review. Microscale Thermophysical Engineering, 6(3): 155-173. https://doi.org/10.1080/10893950290053295

[5] Kandlikar, S.G., Grande, W.J. (2003). Evolution of microchannel flow passages-thermohydraulic performance and fabrication technology. Heat Transfer Eng., 24(1): 3-17. https://doi.org/10.1080/01457630304040

[6] Kandlikar, S.G., Grande, W.J. (2004). Evaluation of single-phase flow in microchannels for high flux chip cooling e thermo-hydraulic performance enhancement and fabrication technology. Heat Transfer Eng., 25(8): 5-16. https://doi.org/10.1080/01457630490519772

[7] Bahrami, M., Yovanovich, M.M., Culham, J.R. (2006). Pressure drop of fully developed, laminar flow in rough microtubes. J. Fluids Eng., 128(3): 632-637. https://doi.org/10.1115/1.2175171

[8] Kosar, A., Peles, Y. (2006). Thermal-hydraulic performance of MEMS-based pin fin heat sink. J. Heat Transfer, 128(2): 121-131. https://doi.org/10.1115/1.2137760

[9] Kosar, A., Mishra, C., Peles, Y. (2005). Laminar flow across a bank of low aspect ratio micro pin fins. J. Fluids Eng., 127(3): 419-430. https://doi.org/10.1115/1.1900139

[10] Bakhti, F.Z., Si-Ameur, M. (2021). Elliptical pin fin heat sink: Passive cooling control. International Journal of Heat and Technology, 39(5): 1417-1429. https://doi.org/10.18280/ijht.390503

[11] Qian, M., Mei, D.Q., Yi, Z.D., Feng, Y.B., Chen, Z.C. (2017). Fluid flow and heat transfer performance in a micro-reactor with non-uniform micro-pin-fin arrays for hydrogen production at low Reynolds number. International Journal of Hydrogen Energy, 42(1): 553-561. https://doi.org/10.1016/j.ijhydene.2016.10.150

[12] Morini, G.L. (2004). Single-phase convective heat transfer in microchannels: A review of experimental results. International Journal of Thermal Sciences, 43: 631-651. https://doi.org/10.1016/j.ijthermalsci.2004.01.003

[13] Jiang, P.X., Xu, R.N. (2007). Heat transfer and pressure drop characteristics of mini-fin structures. International Journal of Heat and Fluid Flow, 28: 1167-1177. https://doi.org/10.1016/j.ijheatfluidflow.2006.11.008

[14] Liu, M.H., Liu, D., Xu, S., Chen, Y.L. (2011). Experimental study on liquid flow and heat transfer in micro square pin fin heat sink. International Journal of Heat and Mass Transfer, 54(25-26): 5602-5611. https://doi.org/10.1016/j.ijheatmasstransfer.2011.07.013

[15] Yang, J., Wang, L., Li, H.Z. (2001). 2-dimensional CFD simulation and correlation development for optimizationof fin heatsinks in electronic cooling. J. of Thermal Science, 10: 363-371. https://doi.org/10.1007/s11630-001-0045-2

[16] Mebarki, G., Rahal, S. (2016). Passive control of two-phase flow thermal instabilities in a vertical tube evaporator. Journal of Thermal Science and Engineering Applications, 8(4): 041008. https://doi.org/10.1115/1.4034092

[17] Tullius, J.F., Tullius, T.K., Bayazitoglu, Y. (2012). Optimization of short micro pin fins in minichannels. Int. J. Heat Mass Transfer, 55(15-16): 3921-3932. https://doi.org/10.1016/j.ijheatmasstransfer.2012.03.022

[18] Yang, D.W., Wang, Y., Ding, G.F., Jin, Z.Y., Zhao, J.H., Wang, G.L. (2017). Numerical and experimental analysis of cooling performance of single-phase array microchannel heat sinks with different pin-fin configurations. Applied Thermal Engineering, 112: 1547-1556. https://doi.org/10.1016/j.applthermaleng.2016.08.211

[19] Eren, M., Caliskan, S. (2016). Effect of grooved pin-fins in a rectangular channel on heat transfer augmentation and friction factor using Taguchi method. International Journal of Heat and Mass Transfer, 102: 1108-1122. https://doi.org/10.1016/j.ijheatmasstransfer.2016.07.005

[20] Hasan, M.I. (2014). Investigation of flow and heat transfer characteristics in micro pin fin heat sink with nanofluid. Applied Thermal Engineering, 63(2): 598-607. https://doi.org/10.1016/j.applthermaleng.2013.11.059

[21] Xu, J.L., Gan, Y.H., Zhang, D.C., Li, X.H. (2005). Microscale heat transfer enhancement using thermal boundary layer redeveloping concept. Int. J. Heat Mass Transfer, 48(9): 1662-1674. https://doi.org/10.1016/j.ijheatmasstransfer.2004.12.008

[22] Chyu, M.K., Hsing, Y.C., Natarajan, V. (1998). Convective heat transfer of cubic fin arrays in a narrow channel. J. Heat Transfer, 120(2): 362-367. https://doi.org/10.1115/1.2841414

[23] Rebay, M., Kakac, S., Cotta, R.M. (Eds.). (2016). Microscale and Nanoscale Heat Transfer: Analysis, Design, and Application (1st ed.). CRC Press. https://doi.org/10.1201/b19261

NOMENCLATURE

C	dimension of pin edge
Cp	specific heat (J/kg K)
Dh	hydraulic diameter (m)
e	dimension of fluid passage
f	friction coefficient
H	pin/channel height
h	convective heat transfer coefficient
L	dissipater length
$\dot{m}$	mass flow rate (kg/mn)
N	number of pins
Nu	Nusselt number
P	absolute pressure (Pa)
q	heat flux density (W/m^2)
Re	Reynolds number
T	temperature (K)
t	temperature fluctuation (K)
ΔT_m	mean temperature difference wall-fluid
U	fluid velocity (m/s)
u	velocity fluctuation (m/s)
W	heat sink width (m)
x,y,z	specials coordinates (m)
ΔP	pressure drop across heat sink (Pa)

Greek symbols

ρ	density (kg/m^3)
μ	dynamic viscosity (kg/m.s)
ν	kinematic viscosity (m^2/s)
λ	thermal conductivity (W/m K)

Subscripts

ave	average
f	fluid
i, j	subscript of
in	inlet
out	outlet
bulk	averaged
ref	Reference
w	wall
c	channel
p	Pin

Abbreviation

RMC	Rectangular Mini-Channel
PFHS	Pin-Fin Heat Sink
VRT	Variable Reference Temperature